Progress In Electromagnetics Research C, Vol. 87, 147–162, 2018

Novel Approach for Vibration Detection Using Indented Radar

Andrew Gigie, Smriti Rani, Arijit Sinharay, and Tapas Chakravarty*

Abstract—Non-contact vibration detection using microwave radar is becoming a popular research area. However, vibration sensing using Doppler radar based measurements suffers from the problem of 'Null point'. In order to mitigate this, traditional designs incorporate phase measurements using Quadrature (I/Q) radar. Such Quadrature radars are not cost effective for large scale indoor deployment scenarios. In this paper, we propose a new configuration of 'Indented Radar'; a system of two single-channel radars offset in space by a path length, which is equivalent to 90 degree phase shift. However, such a system of two independent channels is prone to different imbalances such as amplitude, phase and DC. This work closely examines the imbalance effect on the two-radar system and reports a novel approach that can be used to tackle such imbalance in a two-radar configuration. Our approach yields superior results over other commonly used I/Q algorithms, while measuring vibrational frequencies. Thus, our work can find immense application in both vital sign detection and structural vibration detection use-cases where affordable solution is sought.

1. INTRODUCTION

Microwave Radar Technology has become so versatile these days that it is now being used in various fields rather than detecting only moving targets for use in aviation or space. For example, microwave interferometry is exploited to detect minute vibrations of objects ranging from building [1, 2], bridges, structures [3] to heart movements (i.e., monitoring heart rate) or chest-wall movements (i.e., monitoring breathing rate) [4], or from detecting machine vibrations [5] to human activity. Microwave technology is particularly interesting for its ability to penetrate structures and take measurements from a distance (i.e., in non-contact fashion).

However, like every technology, microwave interferometry [6] suffers from some issues that may corrupt the measurements, if not handled properly. One of such issues arises from the relation between vibrational amplitudes and probing wavelength, while measurements are done through standard radar baseband processing (or sometimes termed as microwave interferometry). If the vibrational amplitude increases in terms of displacement over a certain threshold (compared to the probing wavelength) then the baseband measurement contains harmonics that can often mislead the measurement. This can be managed by maintaining a suitable amplitude vs wavelength ratio. However, the measurement can still suffer from harmonics if measuring around null-points [7]. The situation becomes more problematic in cases where the radar module cannot be fixed at a desirable position (i.e., at optimal point) but requires to take treading on the move (say hand-held unit for detecting machine vibration). Similarly, for use-cases where the subject is also not rigidly bound to a specific point (say non-contact heart-rate or breathing monitoring where people can comfortably stand or sit in front of a fixed radar), the null-point issues may pop-up and can lead to erroneous measurements. Moreover, measurement around null-point not only creates harmonics but also suffers from sharp decrease in sensitivity.

Received 17 July 2018, Accepted 22 September 2018, Scheduled 4 October 2018
* Corresponding author: Tapas Chakravarty (tapas.chakravarty@tcs.com).
The authors are with the TCS Research and Innovation, Kolkata, India.

To overcome such issues related to null-points, people usually use I/Q channels. However, I/Q radars are more expensive and so, people have started experimenting with two single channel radar modules placed side-by-side with some spatial offset to effectively behave as I/Q radar [8]. Here we label this radar system as an "Indented Radar" setup. In this setup, two radar modules have, defined separation both in lateral and longitudinal directions, essentially introducing a physical indentation between them. Although this configuration provides an attractive workaround due to affordability and easy availability of those single channel modules, this configuration is also prone to measurement errors if the information from both modules is not properly combined. If standard approach of combining I and Q channels of an I/Q radar is used as in the case of an Indented Radar, then measurements can suffer from significant errors in certain situations. For example, the most frequently used algorithms for combining I/Q channels like Complex Signal Demodulation (CSD) [9] and Differentiate And Cross Multiply (DACM) [10] will severely fail in certain cases due to amplitude and DC imbalances that are inherently present in the configuration consisting of two independent radar sensors.

The main relevance and usability of an Indented Radar system can be summarized as follows.

- In vibration detection applications such as physiological signals [11] or machine vibration monitoring to detect structural health [1], the Indented Radar can be used to replace I/Q Radar as a cost effective solution.
- In applications such as tracking vehicle speed [12–14], detecting human walking speed, [15] etc. which cut through consecutive null and optimum points the two radars of an Indented Radar system can be considered to have slight shift in transmit frequency thus effectively acting as an Multi frequency Continuous wave radar (MFCW Radar). As mentioned in [16], by calculating the relative phase difference of the output from these radars, we can increase the unambiguous range in a CW radar.
- Multiple radars work as multiple observation points for the same signal. Due to spatial diversity (typically utilized in indoor wireless communication systems), both the radars can jointly subdue the multipath problem besides providing a better coverage area [17].

Thus, Indented Radar potentially performs far better than single channel radars but with accuracy close enough to an actual I/Q radar, at an affordable cost. In this paper, we mainly focus on applications related to vibration detection using Indented Radars, as highlighted in our first bullet point.

In this work, we examine the mismatch problems that can happen in an Indented Radar configuration in detail and propose a suitable approach to combine the information from the two channels for eliminating such pitfalls. The paper is arranged as follows: Section 1 provides a recap on the theory of microwave interferometry while using Indented Radars. Section 2 presents theory and our approach for setting up the Indented Radars. Section 3 briefly explains existing techniques for combining I and Q radar. Section 4 discusses the issues of using CSD and DACM algorithms for the set up for Indented Radars. Next in Section 5, our approach of combining the information from each channel is presented. Next, the experimental set-up is detailed and results are presented in Section 6. Finally, the work is concluded in Section 7.

2. INDENTED RADAR: THEORY AND SETUP

A Continuous Wave (CW) radar transmits a single high frequency continuous wave signal into space. A part of this signal gets backscattered to the receiver after hitting targets. This received echo signal is modulated in phase according to the Doppler principle. Proper demodulation of the received signal can give information about the frequency of the vibrating target.

2.1. Theory

A simplified general block diagram of a CW Radar is shown in Figure 1. The oscillator generates a single tone high frequency signal of frequency f and wavelength λ. This signal $T(t)$ is then transmitted into space using a transmitter antenna (Tx). Let us assume that, the vibrating target, which is at a distance d_0 from the radar, is undulating in simple harmonic motion, $x(t)$ with frequency f. The displacement of the vibrating target modulates the transmitted signal and a part of this signal gets

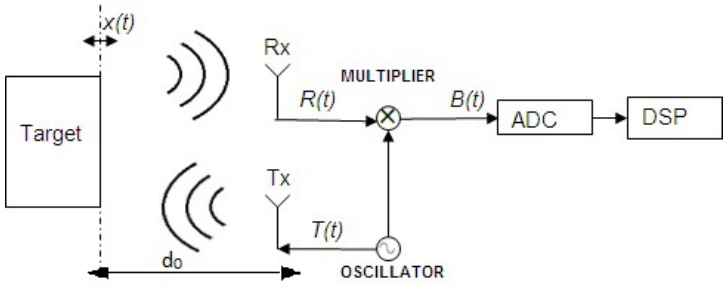

Figure 1. Block diagram of CW radar.

reflected back to the CW radar. This reflected signal is captured by the receiver antenna (Rx). The received echo signal $R(t)$ is then mixed with local oscillator signal coming from the transmitter $T(t)$ and the resultant signal is passed through a low pass filter to filter out the baseband signal $B(t)$. The equation of baseband signal $B(t)$ is as shown in Equation (1) [18].

$$B(t) = \cos\left(\theta_0 + \frac{4\pi x(t)}{\lambda} + \Delta\theta(t)\right) \tag{1}$$

where

$$\theta_0 = \frac{4\pi d_0}{\lambda} \tag{2}$$

and

$$x(t) = A\sin(2\pi f t) \tag{3}$$

$$\Delta\theta(t) = \theta(t) - \theta\left(t - \frac{d_0}{c}\right) \tag{4}$$

Equation (2) represents constant phase due to the fixed distance of the vibrating object from the radar. Equation (3) depicts vibration frequency of the target. $\Delta\theta(t)$ in Equation (4) shows the difference in phase noise from Local Oscillator, for transmitter and receiver respectively. It is usually considered to be negligible for short range application in a quadrature radar [19]. For a body, vibrating at a fixed distance, θ_0 is constant. In an Indented Radar setup, $\Delta\theta(t)$ is no longer negligible, as we are using two separate single channel radars to replicate I/Q Radar.

In Quadrature radar, I and Q outputs are generated by providing a 90 degree phase shift to the oscillator frequency and then mixing with the received echo signal. For an Indented Radar, I and Q outputs have been generated, by spatially separating the two single channel radars by a distance equal to multiples of $\lambda/8$ [8]. A pictorial representation of the setup is shown in Figure 2.

For the indented radar configuration, as shown in Figure 2, Equation (1) is rewritten for both the

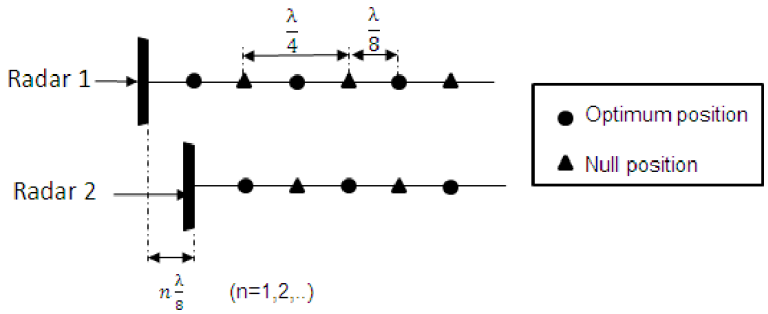

Figure 2. Null and optimum points.

channels as:

$$B_I(t) = \cos\left(\theta_0 + \frac{4\pi x(t)}{\lambda} + \Delta\theta(t)\right) \tag{5}$$

and

$$B_Q(t) = \cos\left(\frac{4\pi(d_0 - \lambda/8)}{\lambda} + \frac{4\pi x(t)}{\lambda} + \Delta\theta(t)\right) \tag{6}$$

Equation (6) may be re-written as

$$B_Q(t) = \cos\left(\frac{\pi}{2} + \theta_0 + \frac{4\pi x(t)}{\lambda} + \Delta\theta(t)\right) \tag{7}$$

$$\text{or} \quad B_Q(t) = \sin\left(\theta_0 + \frac{4\pi x(t)}{\lambda} + \Delta\theta(t)\right) \tag{8}$$

Thus, Equation (5) and Equation (8) form the I and Q channel for the Indented Radar setup.

Now, let us assume that we want to detect composite vibration of the target having two distinct frequencies f_1 and f_2 as shown in Equation (9).

$$x(t) = A_1 \sin(w_1 t) + A_2 \sin(w_2 t) \tag{9}$$

Let us say $\phi = \theta_0 + \Delta\theta(t)$. Then by replacing $x(t)$ in Equation (1) with Equation (9) and writing in the form of Bessel's function [20], we get Equation (11).

$$B(t) = \mathrm{Re}\left(\sum_{n=-\infty}^{\infty} J_n\left(\frac{4\pi A_1}{\lambda}\right) e^{jnw_1 t} \sum_{m=-\infty}^{\infty} J_m\left(\frac{4\pi A_2}{\lambda}\right) e^{jmw_2 t} e^{j\phi}\right) \tag{10}$$

or,

$$B(t) = \sum_{m=-\infty}^{\infty} \sum_{n=-\infty}^{\infty} J_m\left(\frac{4\pi A_2}{\lambda}\right) J_n\left(\frac{4\pi A_1}{\lambda}\right) \cos(nw_1 t + mw_2 t + \phi) \tag{11}$$

From Equation (11), we see that the resultant baseband signal displays the presence of intermodulation frequencies ($f_1 + f_2, f_1 - f_2$, etc.) in addition to the harmonics of vibration frequency ($2f_1, 2f_2$, etc.). Now, depending on the application of interest, we can tune in the value of Bessel coefficients (determined by A_1 and A_2) to determine the amplitude of the harmonic components. Thus, using Equation (11), we can analyze the frequency spectrum of targets having composite vibration.

2.2. Setting up the Indented Radar System

Considering small angle approximation for Equation (1), at an optimum position, the output will be proportional to the vibration displacement of target. However, at null position, the output will be proportional to the square of the vibration displacement. Thus, the output fidelity will depend on the distance between the target and the radar. The harmonic frequencies are generated around null position, which decreases the overall sensitivity of the system. The entire distance in space can be considered to be repetitive bins ranging from Optimum to Null. Since, both the channels are spatially placed at optimum and null position [21], we may call them pseudo I and pseudo Q channel.

In order to conduct our experiments we used two single channel HB100 radars and kept them in such a way that path length between them is approximately, $\lambda/8$. The effect of interference are reduced by placing both the radars in different polarization (one in horizontal and other in vertical polarization) as shown in Figure 3. Ideally, they must behave like a quadrature channel radar. However, because of the effect of phase imbalance due to $\Delta\theta(t)$, this was not observed readily. The radars were then carefully calibrated by finer adjustment in placement to effectively neglect the effect of phase imbalance. This is depicted in Figure 3. This calibration was done by placing a speaker and generating a single tone frequency source (75 Hz) via an amplifier. The radar captures the vibration displacement of the speaker's membrane. The speaker was then placed at a distance such that when one channel (Pseudo I channel) was at null, as shown in Figure 4(a), the other channel (Pseudo Q channel) tends to optimum position, shown in Figure 4(b). At null position, we see the harmonic frequency (150 Hz) to be dominant and at optimum position, we see the fundamental frequency (75 Hz) to be dominant. The final calibrated setup where the effect of phase imbalance is removed is shown Figure 3.

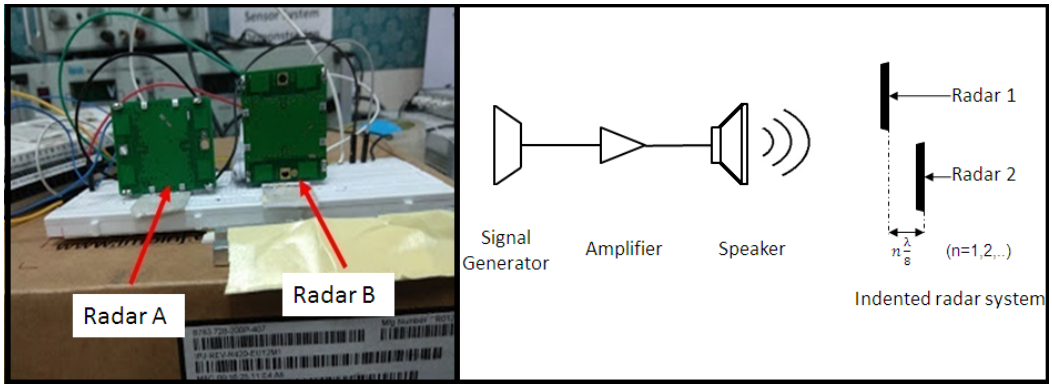

Figure 3. Indented radar setup.

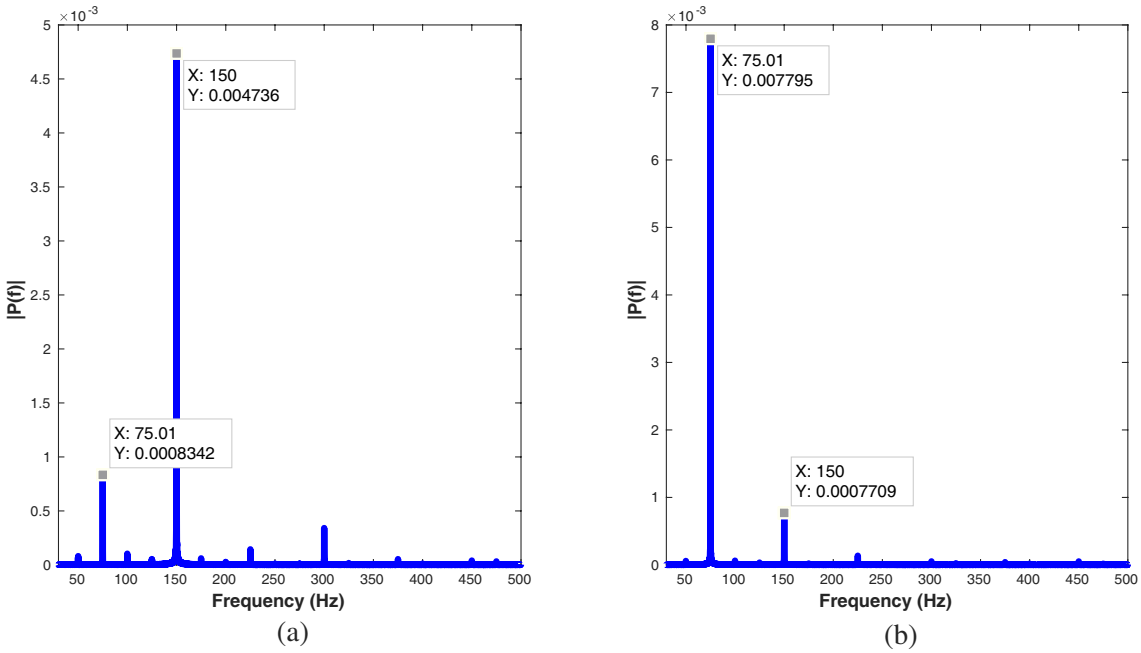

Figure 4. Calibration testing using speaker vibration. (a) Pseudo I channel signal. (b) Pseudo Q channel signa. Pseudo I channel captured second harmonic, suggesting the speaker is near null position and Pseudo Q captured the fundamental frequency, indicating it is near optimum position.

3. PRIOR ART ON COMBINING I AND Q CHANNEL

For ensuring better clarity, we initially explain the existing techniques such as "Complex Signal Demodulation" (CSD) [9] and "Differentiate and Cross Multiply" (DACM) [10] to retrieve the vibration frequency from a Quadrature Radar. We further show the disadvantage of using such techniques in an Indented Radar setup. For an Indented Radar setup, these techniques will become error prone because of mismatches such as amplitude, DC and phase imbalances. Even though there are many ellipse based fitting techniques to compensate for mismatch errors but most of these calibrations is a one time process [22, 23]. To do them repeatedly in real time scenario would be challenging as the mismatch in a Indented Radar would be prominent and unpredictable. Here, we assume that the effect of phase imbalance $\Delta\theta(t)$ was removed in the calibration phase.

3.1. CSD Algorithm

Complex Signal Demodulation (CSD) [9] applies complex Fourier Transform to the I and Q channels to effectively generate the combined output independent of distance between target and radar.

$$B_I(t) + jB_Q(t) = \cos\left(\theta_0 + \frac{4\pi x(t)}{\lambda}\right) + j\sin\left(\theta_0 + \frac{4\pi x(t)}{\lambda}\right) \tag{12}$$

$$B_I(t) + jB_Q(t) = \exp\left(j(\theta_0 + \frac{4\pi x(t)}{\lambda})\right) \tag{13}$$

As seen in Equation (13), the effect of $\exp(j\theta_0)$ is constant in frequency domain and can be removed by removing the average mean. Thus, effectively CSD becomes independent of distance between the radar and target. So, for a given vibrating target, we expect the same frequency spectrum for the CSD output at any distance.

3.2. DACM Algorithm

Differentiate and Cross Multiply (DACM) [10] is a technique that uses both I and Q channels to remove the harmonic content and retrieve the frequency of vibrating target. DACM algorithm is an extension of the traditional Arctangent demodulation technique. In Arctangent demodulation, we perform the arctangent operation on the I and Q channels as shown in Equation (14) to retrieve the linear relation between the output and vibrating frequency of target. Yet, Arctangent demodulation faces the problem of co-domain restriction. In order to solve this problem, DACM algorithm performs differentiation on the arctangent of I and Q channel as shown in Equation (15). Here $\omega(t)$ gives us the velocity of target vibration.

$$\tan^{-1}\left(\frac{B_Q(t)}{B_I(t)}\right) = \theta_0 + \frac{4\pi x(t)}{\lambda} \tag{14}$$

$$\omega(t) = \frac{\partial}{\partial t}\left[\tan^{-1}\frac{B_Q(t)}{B_I(t)}\right] \tag{15}$$

Ideally, the combined output in DACM is free from harmonics, and we can directly retrieve the frequency of vibration signal $x(t)$ from its Fourier Transform.

4. EFFECT ON INDENTED RADAR SYSTEM

For simulating the imbalance effect on the existing algorithms, we assume the target to have a composite vibration of two frequencies (65 Hz and 70 Hz) with equal vibrating displacement of amplitude 0.2 mm (small angle approximation is valid as $\frac{4\pi A_i}{\lambda} < 1$). In such a case, the amplitude of intermodulation frequencies ($f_1 + f_2 = 135$ Hz) would be more than the harmonics ($2f_1 = 130$ Hz and $2f_2 = 140$ Hz). In order to prove this, consider a target vibrating with small amplitude at null point. Then, Equation (1) can be re-expressed as

$$B(t) = 1 - \frac{1}{2}\left(\frac{4\pi x(t)}{\lambda} + \Delta\theta(t)\right)^2 \tag{16}$$

Substituting Equation (9) in Equation (16), with $A_1 \approx A_2 \approx A$ and using basic trigonometric properties, we can rewrite Equation (16) as Equation (17). Here, we neglect the effect of phase imbalance.

$$B(t) = 1 - \frac{1}{2}\left(\frac{4\pi A}{\lambda}\right)^2\left[1 - \frac{1}{2}\cos(2w_1 t) - \frac{1}{2}\cos(2w_2 t) - \cos((w_1 + w_2)t) + \cos((w_1 - w_2)t)\right] \tag{17}$$

Thus, from Equation (17), we observe that amplitude of intermodulation frequency, i.e., $w_1 + w_2$, (65 Hz + 70 Hz = 135 Hz) is more dominant than the individual second harmonic, i.e., $2w_1$ or $2w_2$ (130 Hz or 140 Hz).

The transmitting frequency is 10.525 GHz, and the target is at a distance such that when one channel is at optimum position, the other channel is at null position. These parameters were then used to represent $x(t)$ as shown in Equation (9).

4.1. CSD

The ideal CSD equation is shown in Equation (13). In case of a calibrated Indented Radar setup, amplitude and DC imbalances are bound to happen in real time. By simulating different scenarios of mismatch (amplitude and DC), we found that the effect of amplitude mismatch is significant. Hence, the effect of amplitude imbalance has been examined more closely, when CSD technique is applied. Thus, Equation (13) should be modified as Equation (18).

$$B_I(t) + jB_Q(t) = A_i \cos\left(\theta_0 + \frac{4\pi x(t)}{\lambda}\right) + jA_q \sin\left(\theta_0 + \frac{4\pi x(t)}{\lambda}\right) \tag{18}$$

where A_i and A_q represent the amplitude mismatch between the two channels. Ideally, CSD algorithm gives the same frequency spectrum at any distance for the combined output and we expect the Signal strength (SNR) at null position to be far less than optimum position. However, due to amplitude mismatch, this may not always be true. The effect of amplitude imbalance on CSD output is obtained by simulating Equation (18). Here, the value of amplitude mismatch (A_i, A_q) is given by observing the outputs obtained from actual experiment ($A_i = 0.016\,\text{V}$ and $A_q = 0.01\,\text{V}$). Figure 5(a) and Figure 5(b) show the frequency spectrum of I and Q channels at a particular distance. Figure 5(c) shows the ideal frequency spectrum without amplitude imbalance and Figure 5(d) shows the frequency spectrum of CSD having amplitude imbalance. As seen from Figure 5(d), the amplitude imbalance gave relatively more signal strength to the harmonics.

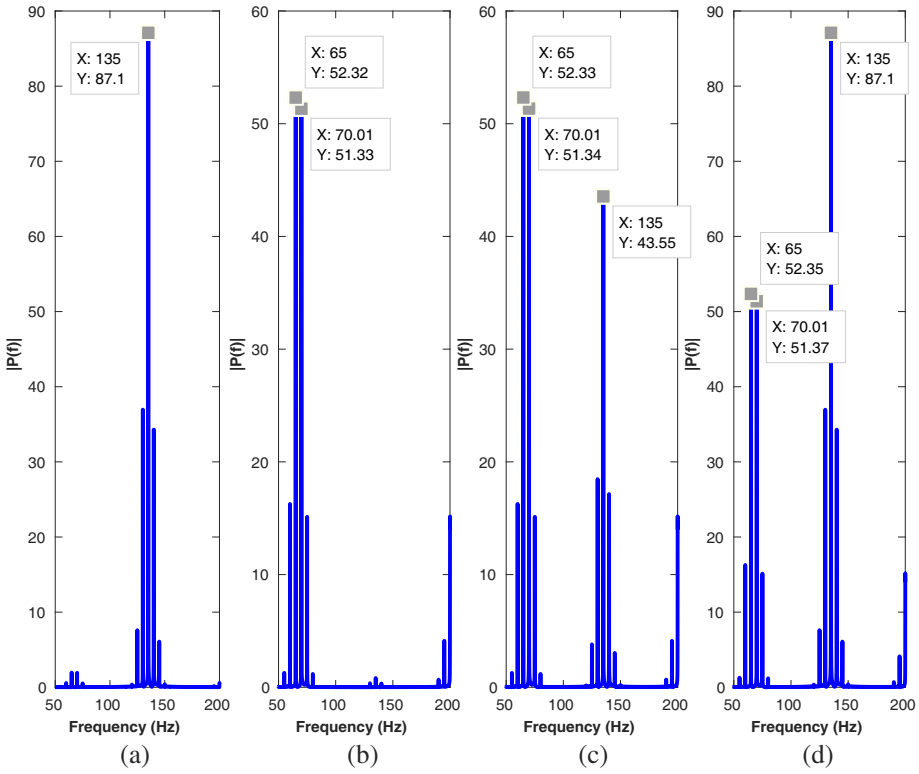

Figure 5. Simulated effect of amplitude imbalance on CSD Algorithm. Frequency spectrum of (a) I channel, (b) Q channel, (c) CSD technique without amplitude imbalance, (d) CSD technique with amplitude imbalance. It is seen from (d), that harmonic content has more signal strength than fundamental.

4.2. DACM

For an Indented Radar system, Equation (15) should be modified as it would be subject to Amplitude and DC imbalance. By simulating different cases, it is observed that in DACM algorithm the effect

of DC offset is more crucial than amplitude imbalance and other factors, as addressed in [24] and [9]. Thus, considering the DC offset imbalance, Equation (15) gets modified to Equation (19).

$$\frac{\partial}{\partial t}\left[\tan^{-1}\frac{B_Q(t)}{B_I(t)}\right] = \frac{\partial}{\partial t}\left[\tan^{-1}\left(\frac{DC_i + \theta_0 + \dfrac{4\pi x(t)}{\lambda}}{DC_q + \theta_0 + \dfrac{4\pi x(t)}{\lambda}}\right)\right] \tag{19}$$

As seen from Equation (19), now it is not possible to directly retrieve the frequency of vibration signal $x(t)$ from its frequency spectrum, and the combined output would become unpredictable. The effect of DC imbalance on the combined output of DACM is obtained by simulating Equation (19). A mean removal filter has been used for DC removal. Thus, a time varying DC imbalance was introduced in one of the channels. For the first half of the entire time duration of the signal, $DC_i = 0.0165\,\text{V}$ and $DC_q = 0.01\,\text{V}$. For the second half $DC_i = 0.01\,\text{V}$ and $DC_q = 0.01\,\text{V}$. Figure 6(a) and Figure 6(b) show the frequency spectrum of I and Q channels at a particular distance. Figure 6(c) shows the ideal frequency spectrum of DACM algorithm, without DC imbalance and Figure 6(d) shows the frequency spectrum of DACM algorithm, with DC imbalance. As seen from Figure 6(d), the DC imbalance in the two channels led to the generation of unwanted frequencies of significant amplitude. This may lead to unpredicatable frequency measurements in certain scenarios. Thus, DACM algorithm can only be taken in a very accurately calibrated dual channel IQ Radar setup. In an Indented Radar setup which is bound to have irregularities, it is thus impractical to go for such an approach.

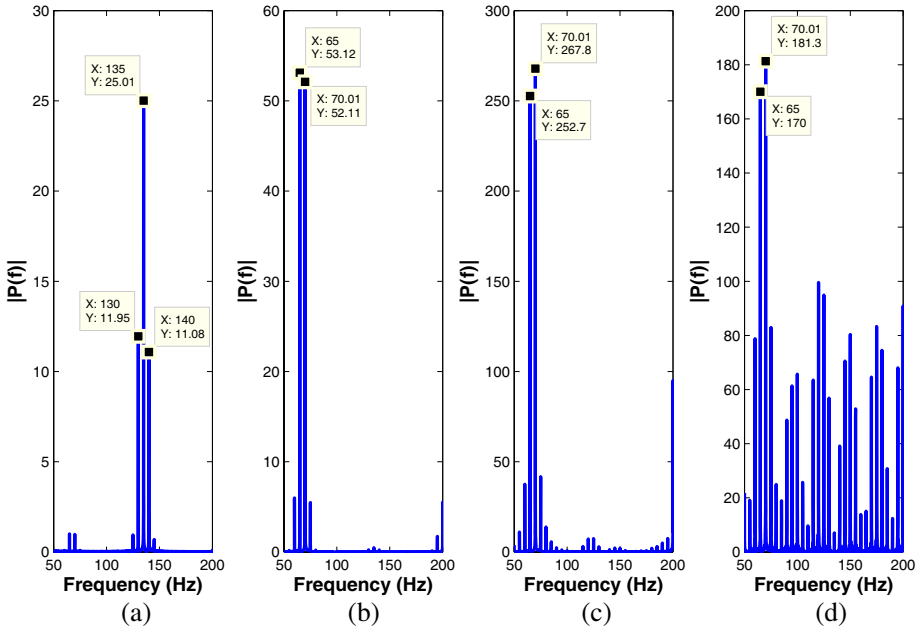

Figure 6. Simulated effect of DC imbalance on DACM Algorithm. Frequency spectrum of (a) I channel, (b) Q channel, (c) DACM technique without DC imbalance, (d) DACM technique with DC imbalance. Comparison between (c) and (d) suggests that DC imbalance causes the energy from the fundamental peaks to spill over to number of other frequency bins.

5. OUR APPROACH

As mentioned earlier, with two entirely separate sets of Transmitters, Receivers and Local Oscillators, an Indented Radar system is bound to suffer from amplitude (A_i and A_q) and DC imbalance (DC_i and DC_q). These effects make the output baseband signal uncertain. To overcome the said issues, we came up with a novel approach of combining supervised method with complex signal demodulation. We term it as Supervised Complex Signal Demodulation (SCSD).

Most vibrating mechanisms are band limited. For instance, for a healthy individual, physiological signals, such as breathing rate [25] and heart rate are band limited to 0.2–0.4 Hz and 1–2 Hz, respectively. Similarly, machines also vibrate in a particular frequency range. Hence, we know the fundamental frequency band, as well as, the corresponding harmonics. In this paper, we mainly focus on composite vibration detection of two distinct frequencies. This is taken in order to consider the effect of intermodution frequencies as well. Now, we create a simulated model of the system using Equation (11) and generate the frequency spectrum of composite vibration. The entire distance in space can be considered to be repetitive bins ranging from Optimum to Null. Each such bin is then further subdivided into five classes. These classes are labelled as "null", "better null", "middle", "better optimum" and "optimum". These classes are selected such that the frequency pattern is distinct in each of them. At any distance, either pseudo I channel or pseudo Q channel captures a better estimation of the fundamental frequencies present in the vibrating system. Thus, based on the frequency pattern of the input signal, we create a supervised learning model using weighted KNN algorithm [26] to allocate the closest resemblance class for the input signal. The features for the model are based on the location of peaks and the ratio of the relative peak to peak distance between them. The training data for the model is generated in Matlab using the steps mentioned below.

(i) Select a particular bin ranging from Optimum position to Null position (Indirectly, fixing a particular distance).

(ii) Depending upon the application, decide on the frequency band of operation (Indirectly, fixing a frequency bandwidth).

(iii) Depending upon the distinct frequency spectrum (function of distance), we divide the bin into five classes and Annotate the ground truth with corresponding class labels.

(iv) For a particular class, simulate Equation (11) for incremental steps of all frequencies in the frequency range and small incremental distances of that particular class.

(v) Using Step (iv) generate features such as location of peaks and peak to peak ratio from frequency spectrum plots.

(vi) Use these features to train the supervised learning model using weighted KNN. Repeat steps (iv) and (v) for all classes ("null", "better null", "middle", "better optimum" and "optimum") of a particular bin.

Currently, we generate the model by analyzing the frequency spectrum of composite vibration on a single channel as explained in Equation (11). Thus in the testing phase, feature sets obtained from the experimental data of pseudo I and Q channel in the Indented Radar system is fed separately to the model. After discerning the label, the weighted KNN model assigns α and β values to channels I and Q, respectively. Nearer the frequency pattern is, to the optimum bin, more is the α or β value. The classes and their corresponding α or β value are shown in Table 1.

$$B(t) = \alpha I + j\beta Q; \tag{20}$$

After assigning α and β values for both the channels, the outputs are combined using Equation (20). A block diagram is shown in Figure 7 explaining the above process.

Table 1. Assigned values of α or β.

Class	Null	Better Null	Middle	Better Optimum	Optimum
α or β	0	0.25	0.5	0.75	1

This method addresses the problem of Amplitude and DC offset variations that can happen in the proposed system, as the model considers both the channels independent of each other while assigning the class label and more weight is given to the signal having resemblance to the optimum position.

In order to explain the above model, consider a scenario, where a machine is vibrating with a composite vibration of two frequency components. For experimental analysis, a speaker can be fed

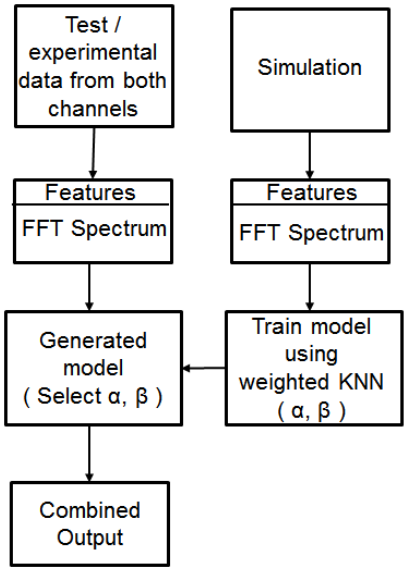

Figure 7. Supervised CSD block diagrams.

with a multi-tone source, to emulate composite vibration in machines. Here, the speaker would be fixed, but the Indented Radar system is a movable hand-held device. In this case, the distance between Indented Radar and speaker is not fixed, but the combined output should be independent of distance. The data for training the model is generated in this scenario by simulating Equation (11). We first select a bin from optimum to null and then divide the bin into 5 classes (annotated ground truth), we then incrementally train our model for the desired frequency range at different distances within each class. For example, let's feed an audio signal to the speaker with two frequency components, f_1 (65 Hz) and f_2 (70 Hz) of equal amplitude. The amplitude value of the audio source is given so that the simulated frequency spectrum using Equation (11) ($A_1 = 0.3$ mm, $A_2 = 0.28$ mm, ($A_1 \approx A_2$)) was similar to the actual experimental frequency spectrum. Thus using Equation (11), the main peak frequency components expected are, the fundamental frequencies f_1 (65 Hz), f_2 (70 Hz) and harmonic frequencies such as $2f_1$ (130 Hz), $2f_2$ (140 Hz), $f_1 + f_2$ (135 Hz), etc. As explained using Equation (17), when $A_1 \approx A_2$, we observe that intermodulation frequency (135 Hz) would have more amplitude than other harmonics (130 Hz and 140 Hz) in the frequency spectrum. The typical frequency spectrum for the five annotated ground truth classes is depicted in Figure 8. The data from the two channels of the Indented Radar system, is then fed to this trained model and depending upon the class label the model allocates, the values of α and β. The combined output from SCSD will always show a pattern closer to the optimum pattern. Thus, creating an output relatively independent of distance. This is further portrayed in Section 6.

For another use-case, consider physiological signals from the movement of the chest wall of human body. It consists of a composite vibration of breathing and heartbeat. We know that the typical Breathing rate normally ranges from 0.2 Hz to 0.4 Hz (12 to 24 beats/minute) and displacement amplitude of chest for breathing has a peak to peak displacement of 2 mm to 6 mm [27]. As the displacement amplitude of heart beat is very less than breathing. In Equation (11) we can assume that $A_1 \gg A_2$, hence the two main frequency component that is expected at any distance is the fundamental frequency between 0.2 Hz to 0.4 Hz and the second harmonic of breathing, generally in the range of 0.4 Hz to 0.8 Hz. Thus, similar to the approach taken for machine vibration case, a model can be made by looking into the frequency spectrum generated using Equation (11).

Thus, for composite vibration using Equation (11), a model can be made corresponding to the signatures and frequency band pertaining to the application. After that, a supervised approach, as mentioned above can be used along with the existing CSD algorithm.

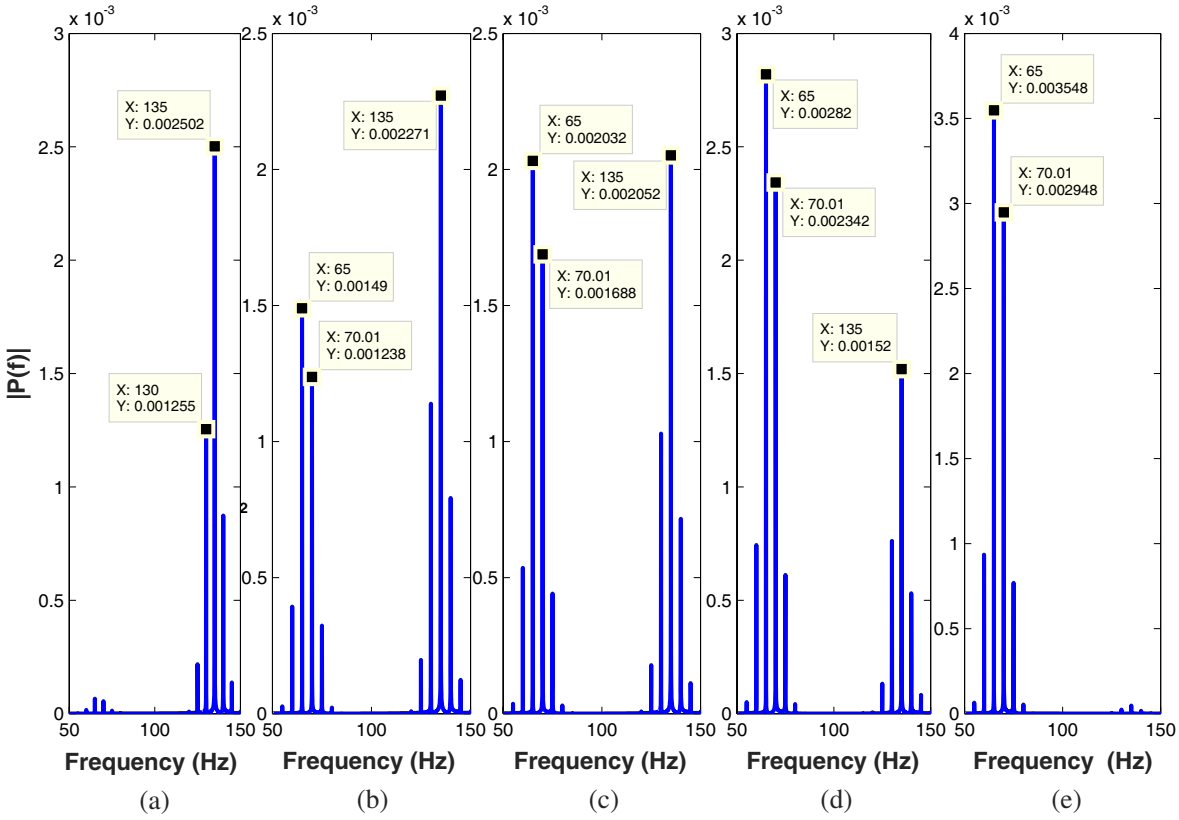

Figure 8. Frequency spectrum in different classes for a single channel radar. (a) Null class. (b) Better Null class. (c) Middle class. (d) Better Optimum class. (e) Optimum class for machine vibration. Distinct Frequency spectrum pattern is observed for different classes ("null", "better null", "middle", "better optimum" and "optimum").

6. EVALUATION OF VIBRATION DETECTION

6.1. Experimental Setup

Experiments were performed with the help of Indented Radar system, as described in Section 2. Data were collected with the help of LabView. To check the ruggedness of the system, no special care was taken to shield the system from environmental noise and electromagnetic interference. The data from both the channels are fed to the model explained in Section 5. In order to test the competence of our approach with respect to existing algorithms, data has been collected in two different scenarios.

6.1.1. Machine Vibration Monitoring

To emulate the behaviour of a vibrating membrane, a speaker is an apt choice. An audio source having composite vibration of two frequencies is fed to the speaker. The frequency bandwidth considered was 60 Hz to 80 Hz and model was generated for that frequency range, with a frequency step of 1 Hz.

As a test case, the diaphragm of the speaker is vibrated at a combined frequency of 65 and 70 Hz. This reveals various intermodulation and harmonic effects of the two frequencies. The outputs from the Indented Radar system was sampled at 1 KHz using NI DAQ board USB-6216. In order to compare SCSD with CSD, data were collected by incrementally moving the speaker in 20 steps of 0.2 cm each, away from the speaker. The duration of measurement at each distance was around 60 seconds. The buffered data were fed to the simulated model. Based on the frequency pattern, the simulated model assigns α and β. The complete setup for the experiment was conducted is shown in Figure 9.

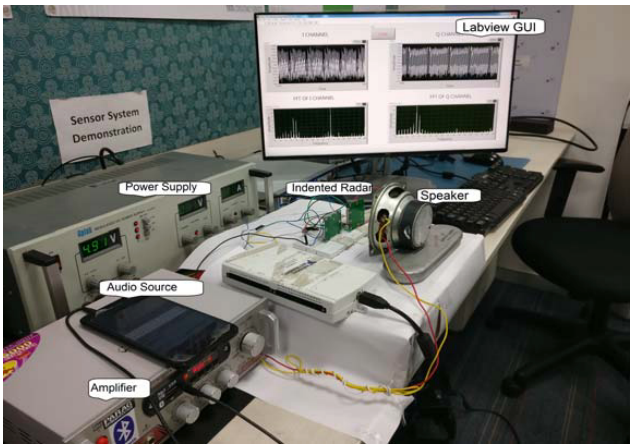

Figure 9. Machine vibration setup.

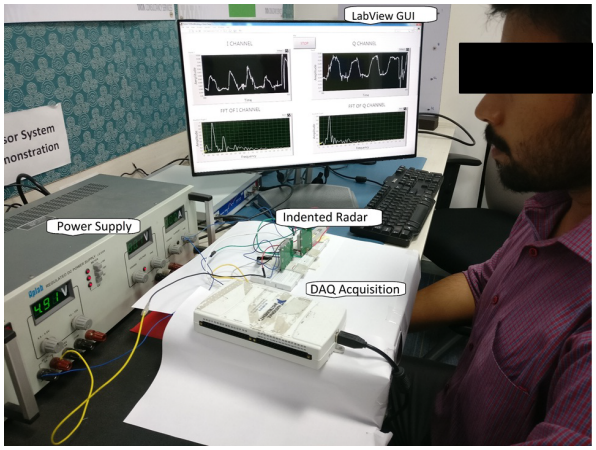

Figure 10. Physiological sensing set up.

6.1.2. Physiological Monitoring

For validating SCSD for physiological signals, the simulation model was generated to have a bandwidth of 0.2 Hz to 0.4 Hz (corresponding to normal breathing rate). Experiments were then performed on one of the authors of this paper. The setup shown in Figure 10 was used to collect data. The subject was seated at a distance of around 0.3 m away from the Indented Radar system and asked to restrict movement while breathing. The subject was wearing a formal shirt. 20 reading were taken in such an arrangement. Responses from the Indented Radar system were taken at a sampling rate of 50 Hz via an NI DAQ board USB-6216, through LabView.

6.2. Results and Discussion

In this section, we compare the accuracy of our approach with one of the existing techniques — complex signal demodulation (CSD). Both the techniques use the same data sets.

Figure 11 shows one of the observations for machine vibration monitoring. Ideally, the signal close to the null position should have less SNR than the signal near optimum. However, in an Indented Radar setup, amplitude imbalance can give more strength to the signal near null position. As seen, pseudo I channel (Figure 11(a)) was near to the null position and had signal strength comparable to the pseudo Q channel Figure 11(b), which was near optimum position. Thus, the combined CSD output in Figure 11(c) was incorrect and had more harmonic content. As can be seen from Figure 11(d), SCSD gives more weightage to the channel near optimum position. Hence, the effect of amplitude imbalance was suppressed.

Figure 12 shows the error graph for 20 different observation points in machine vibrations scenario. The error is computed by taking a ratio of the amplitude of the dominant frequency (except the fundamental) to the amplitude of the fundamental frequency in the combined signal (D-F ratio). For this case, the fundamental frequency is 65 or 70 Hz and the dominant frequency, excluding the fundamental is 135 Hz. This D-F ratio would be small if the combined signal is close to the optimum. Ideally, CSD should give a constant D-F ratio at any distance as the pattern is independent of distance. However as seen from Figure 12, in some cases because of amplitude imbalance this ratio is very high. Using SCSD technique it is seen that the D-F ratio is very less and is comparatively better than CSD in all the cases.

Physiological signals have very low amplitude band-limited signals. Adding up the harmonics can lead to false detection of the vital signs. 20 sets of data were collected using the setup explained in Section 6.1.2. Figure 13(a) and Figure 13(b) show the two channels for one of such observations. The observed Breathing rate for the subject in this observation was 18 breaths per minute. As seen from the figure, the fundamental breathing rate for the subject was around 0.29 Hz (18 breathes/minute) and the corresponding harmonic frequency was around 0.59 Hz. Due to amplitude imbalance, the harmonic frequency had signal strength comparable to the fundamental frequency. Hence, for CSD technique in

Figure 13(c), both harmonic and fundamental frequencies are almost equal. However depending upon its frequency spectrum pattern, SCSD technique detected I channel as in the "better optimum" class and Q channel was labelled as "better null". Hence weights were accordingly given to both channels to suppress the effect of amplitude imbalance. This is clearly visible in Figure 13(d).

Figure 14 plots the D-F ratio for physiological signals of 20 different sets of data for a human subject. In this case, excluding the fundamental breathing frequency, the second harmonic frequency of respiration is the dominant frequency. For the case of vital signs, the amplitude of heart rate frequency

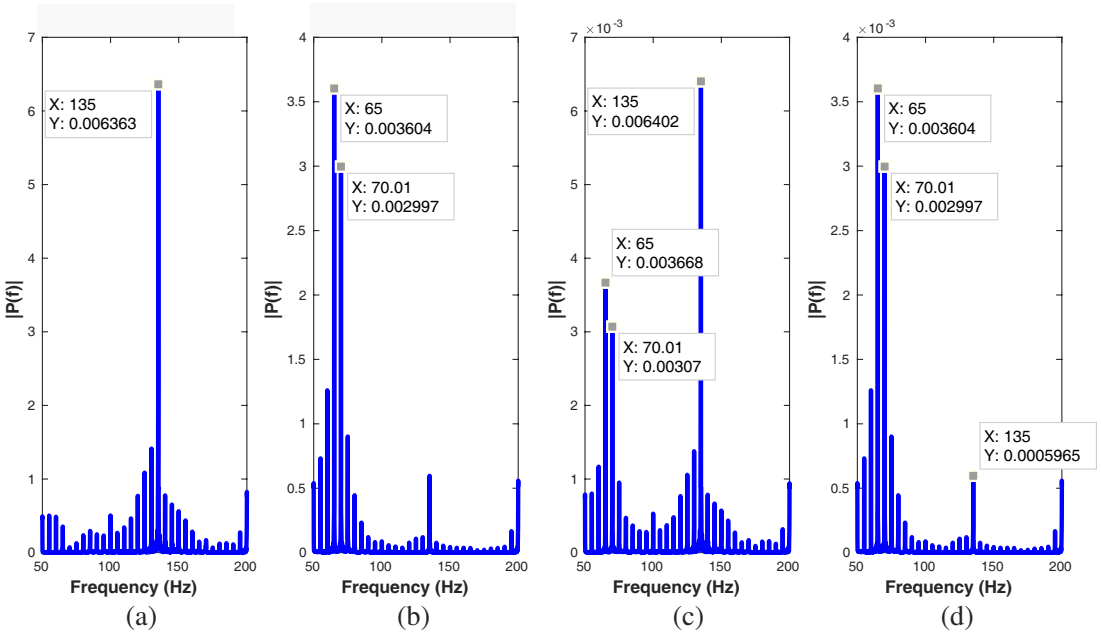

Figure 11. Frequency spectrum of (a) Pseudo I channel, (b) Pseudo Q channel, (c) CSD technique, (d) SCSD technique in Machine vibration monitoring. Fundamental frequencies (65 Hz and 70 Hz) are the prominent peaks for SCSD technique. From (c), it is seen that the intermodulation frequency (13 Hz) gains more signal power, whereas in (d) SCSD gives more weightage to the the fundamental frequency.

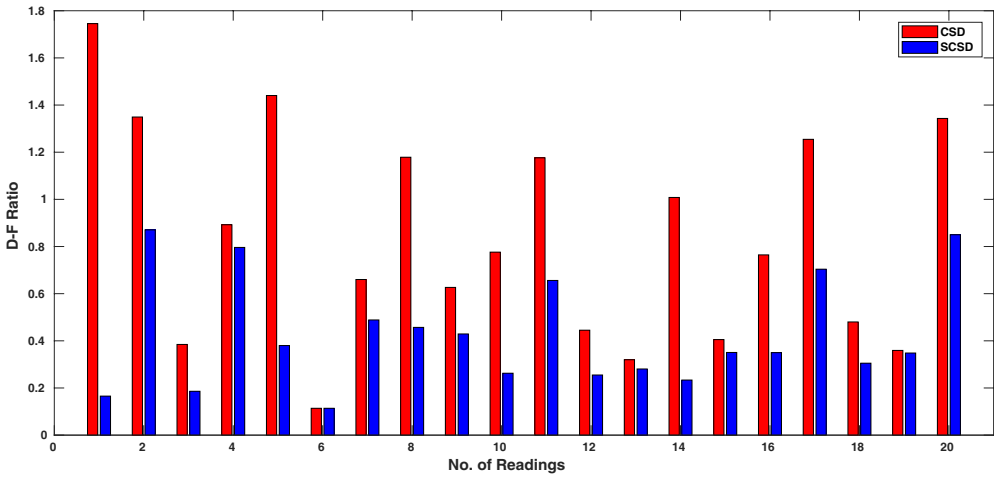

Figure 12. Comparison between CSD technique and SCSD technique in Machine Vibration. Here, DF Ratio refers to the ratio of amplitude of dominant frequency (except the fundamental-135 Hz) to fundamental (65 Hz or 70 Hz). Ideally, it should be less than 1.

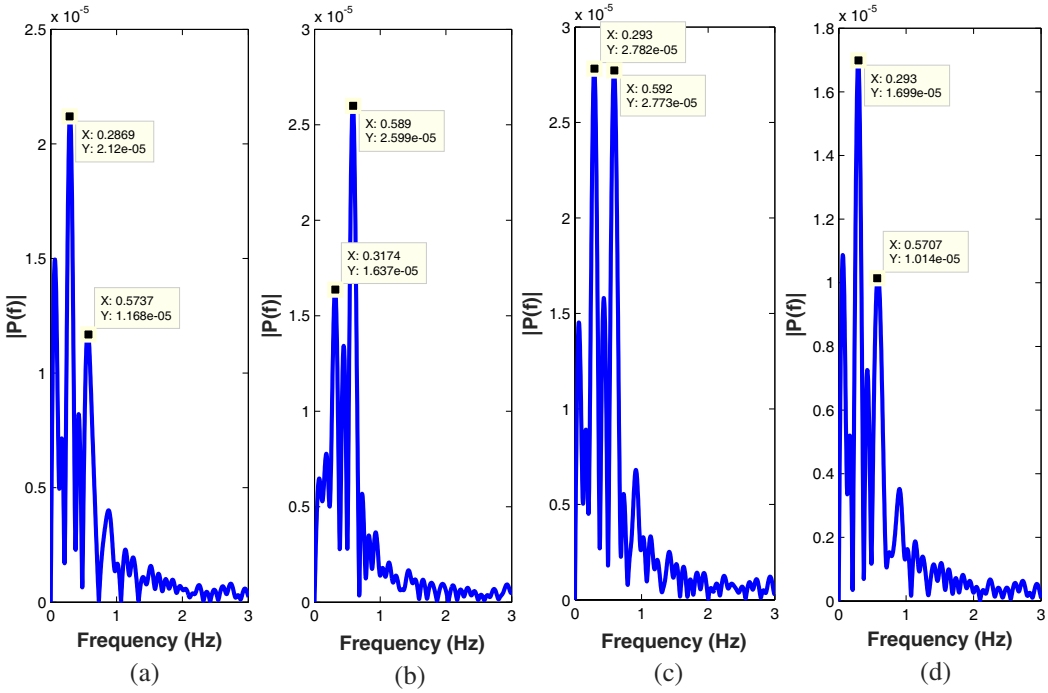

Figure 13. Frequency spectrum of (a) Pseudo I channel, (b) Pseudo Q channel, (c) CSD technique, (d) SCSD technique in physiological Monitoring. For CSD technique (c), both the fundamental and harmonic frequencies have almost equal power, whereas, for SCSD technique (d) fundamental frequency is clearly visible.

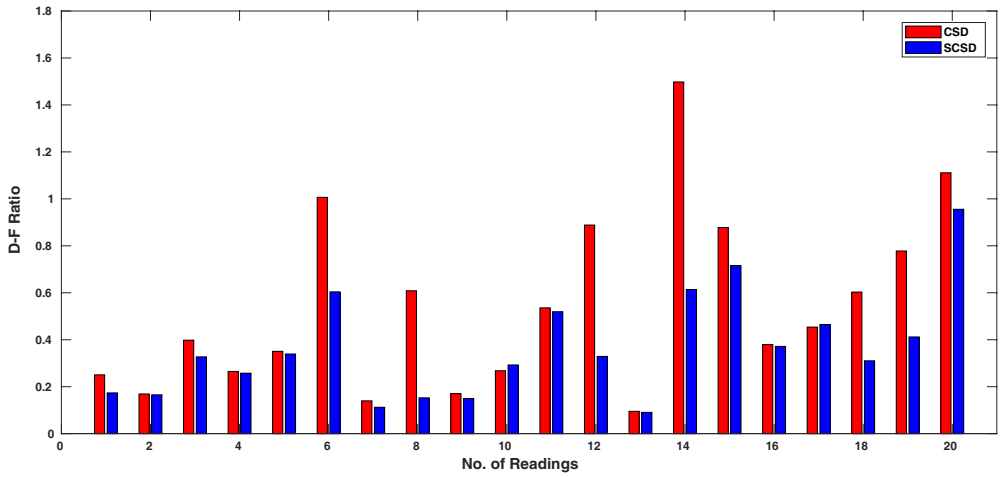

Figure 14. Comparison between CSD technique and SCSD technique in Physiological Monitoring. Here, D-F Ratio denotes the ratio of dominant frequency (except the fundamental) to fundamental frequency. Ideally, it should be less than 1.

would be very less than the respiration rate frequency. Consequently, the higher order harmonics of breathing comes in the Heart beat range. Hence, the combined output should have harmonic content as less as possible to detect heart rate. We further observe that for almost all observation points, SCSD scores far better than CSD in terms of finding the fundamental frequencies of vibration. Thus ensuring that the harmonic content using SCSD technique would be minimum.

7. CONCLUSIONS

Our work discusses in length the issues of using Indented Radars for vibration measurements. Both physiological and pure mechanical vibrations are examined closely. Our results clearly show that standard I/Q algorithms like CSD or DACM often fail to detect actual vibrational frequencies when applied on Indented Radars. Moreover, our approach of fusing information, through supervised approach, from the individual channels of radars proves to be accurate and superior to CSD or DACM when used in indented configurations. This provides an affordable means for exploiting microwave interferometry, through indented radar configuration, to overcome the null-point issues while monitoring vibrations from a distance. Thus, our work can find immense applications in non-contact vibration detection use-cases, especially, where the radar to subject distance is not fixed (i.e., monitoring with hand-held radars). Currently, both channels are fed independently to the trained model to generate α and β. This however limits the frequency bandwidth that can be trained. In future work, we intend to utilize both channel characteristics concurrently to generate more features, in order to generalize this solution to scale all frequencies.

REFERENCES

1. Pieraccini, M., M. Fratini, F. Parrini, G. Macaluso, and C. Atzeni, "High-speed cw step-frequency coherent radar for dynamic monitoring of civil engineering structures," *Electronics Letters*, Vol. 40, No. 14, 907–908, 2004.
2. Luzi, G., O. Monserrat, and M. Crosetto, "The potential of coherent radar to support the monitoring of the health state of buildings," *Research in Nondestructive Evaluation*, Vol. 23, No. 3, 125–145, 2012.
3. Moll, J., J. Simon, M. Malzer, V. Krozer, D. Pozdniakov, R. Salman, M. Durr, M. Feulner, A. Nuber, and H. Friedmann, "Radar imaging system for in-service wind turbine blades inspections: Initial results from a field installation at a 2 mw wind turbine," *Progress In Electromagnetics Research*, Vol. 162, 51–60, 2018.
4. Kranjec, J., S. Begus, J. Drnovsek, and G. Gersak, "Novel methods for noncontact heart rate measurement: A feasibility study," *IEEE Transactions on Instrumentation and Measurement*, Vol. 63, No. 4, 838–847, 2014.
5. Raffo, A., S. Costanzo, and G. Di Massa, "Software defined doppler radar as a contactless multipurpose microwave sensor for vibrations monitoring," *Sensors*, Vol. 17, 115, Jan. 2017.
6. Ivanov, E. N., M. E. Tobar, and R. A. Woode, "Microwave interferometry: Application to precision measurements and noise reduction techniques," *IEEE Transactions on Ultrasonics, Ferroelectrics, and Frequency Control*, Vol. 45, No. 6, 1526–1536, 1998.
7. Park, B.-K., S. Yamada, O. Boric-Lubecke, and V. Lubecke, "Single-channel receiver limitations in doppler radar measurements of periodic motion," *2006 IEEE Radio and Wireless Symposium*, 99–102, IEEE, 2006.
8. Rahman, A., E. Yavari, A. Singh, V. Lubecke, and O. B. Lubecke, "Single-channel radar fusion for quadrature life-sign doppler radar," *2016 IEEE/ACES International Conference on Wireless Information Technology and Systems (ICWITS) and Applied Computational Electromagnetics (ACES)*, 1–3, IEEE, 2016.
9. Li, C. and J. Lin, "Complex signal demodulation and random body movement cancellation techniques for non-contact vital sign detection," *2008 IEEE MTT-S International Microwave Symposium Digest*, 567–570, IEEE, 2008.
10. Wang, J., X. Wang, L. Chen, J. Huangfu, C. Li, and L. Ran, "Noncontact distance and amplitude-independent vibration measurement based on an extended dacm algorithm," *IEEE Transactions on Instrumentation and Measurement*, Vol. 63, No. 1, 145–153, Jan. 2014.
11. Obeid, D., S. Sadek, G. Zaharia, and G. E. Zein, "Doppler radar for heartbeat rate and heart rate variability extraction," *2011 E-Health and Bioengineering Conference (EHB)*, 1–4, Nov. 2011.
12. Roy, A., N. Gale, and L. Hong, "Automated traffic surveillance using fusion of doppler radar and video information," *Mathematical and Computer Modelling*, Vol. 54, No. 1, 531–543, 2011.

13. Alessandretti, G., A. Broggi, and P. Cerri, "Vehicle and guard rail detection using radar and vision data fusion," *IEEE Transactions on Intelligent Transportation Systems*, Vol. 8, No. 1, 95–105, Mar. 2007.
14. Jeng, S. L., W. H. Chieng, and H. P. Lu, "Estimating speed using a side-looking single-radar vehicle detector," *IEEE Transactions on Intelligent Transportation Systems*, Vol. 15, No. 2, 607–614, Apr. 2014.
15. Gürbüz, S. Z., W. L. Melvin, and D. B. Williams, "Detection and identification of human targets in radar data," *Signal Processing, Sensor Fusion, and Target Recognition XVI*, Vol. 6567, 65670I, International Society for Optics and Photonics, 2007.
16. Anderson, M. G. and R. L. Rogers, "Micro-doppler analysis of multiple frequency continuous wave radar signatures," *Radar Sensor Technology XI*, Vol. 6547, 65470A, International Society for Optics and Photonics, 2007.
17. Fishler, E., A. Haimovich, R. S. Blum, L. J. Cimini, D. Chizhik, and R. A. Valenzuela, "Spatial diversity in radars - models and detection performance," *IEEE Transactions on Signal Processing*, Vol. 54, No. 3, 823–838, 2006.
18. Gu, C., "Short-range noncontact sensors for healthcare and other emerging applications: A review," *Sensors*, Vol. 16, No. 8, 1169, 2016.
19. Droitcour, A. D., O. Boric-Lubecke, V. M. Lubecke, J. Lin, and G. TA Kovacs, "Range correlation and i/q performance benefits in single-chip silicon doppler radars for noncontact cardiopulmonary monitoring," *IEEE Transactions on Microwave Theory and Techniques*, Vol. 52, No. 3, 838–848, 2004.
20. Skolnik, M. I., "Introduction to radar," *Radar Handbook*, 2, 1962.
21. Li, C., V. M. Lubecke, O. Boric-Lubecke, and J. Lin, "A review on recent advances in doppler radar sensors for noncontact healthcare monitoring," *IEEE Transactions on Microwave Theory and Techniques*, Vol. 61, No. 5, 2046–2060, May 2013.
22. Singh, A., X. Gao, E. Yavari, M. Zakrzewski, X. H. Cao, V. M. Lubecke, and O. Boric-Lubecke, "Data-based quadrature imbalance compensation for a cw doppler radar system," *IEEE Transactions on Microwave Theory and Techniques*, Vol. 61, No. 4, 1718–1724, Apr. 2013.
23. Zakrzewski, M., A. Singh, E. Yavari, X. Gao, O. Boric-Lubecke, J. Vanhala, and K. Palovuori, "Quadrature imbalance compensation with ellipse-fitting methods for microwave radar physiological sensing," *IEEE Transactions on Microwave Theory and Techniques*, Vol. 62, No. 6, 1400–1408, 2014.
24. Nosrati, M. and N. Tavassolian, "High-accuracy heart rate variability monitoring using doppler radar based on gaussian pulse train modeling and ftpr algorithm," *IEEE Transactions on Microwave Theory and Techniques*, Vol. 66, No. 1, 556–567, Jan. 2018.
25. Liu, Z., L. Liu, and B. Barrowes, "The application of the Hilbert-Huang transform in through-wall life detection with uwb impulse radar," *PIERS Online*, Vol. 6, No. 7, 695–699, 2010.
26. Wu, X., V. Kumar, J. R. Quinlan, J. Ghosh, Q. Yang, H. Motoda, G. J. McLachlan, A. Ng, B. Liu, S. Yu Philip, et al., "Top 10 algorithms in data mining," *Knowledge and Information Systems*, Vol. 14, No. 1, 1–37, 2008.
27. Lazaro, A., D. Girbau, and R. Villarino, "Analysis of vital signs monitoring using an IR-UWB radar," *Progress In Electromagnetics Research*, Vol. 100, 265–284, 2010.